THESIS

FABRICATION OF SLIPPERY TEXTURED AND SLIPPERY NON-TEXTURED SURFACES

Submitted by

Matthew Cackovic

Department of Chemical and Biological Engineering

In partial fulfillment of the requirements

For the Degree of Master of Science

Colorado State University

Fort Collins, Colorado

Fall 2018

Master's Committee:

Advisor: Arun K. Kota

Ketul Popat
Travis Bailey

ABSTRACT

FABRICATION OF SLIPPERY TEXTURED AND SLIPPERY NON-TEXTURED SURFACES

Slippery surfaces, i.e., surfaces that have high droplet mobility and low lateral adhesion for liquid droplets, have a wide range of application such as condensation heat transfer, anti-corrosion, lab-on-chip devices, etc. These surfaces can be categorized into smooth slippery surfaces and super-repellant textured slippery surfaces.

In this work, we fabricated super-repellant textured superomniphobic paper surfaces. We developed a simple and facile method to fabricate superomniphobic paper surface by growing silicone nanofilaments on a glass microfiber paper surface before imparting low solid surface energy to give the surface the appropriate texture and chemistry. We characterized the performance of our surface and demonstrated our surfaces potential as a lab-on-chip type device. We showed high droplet transport rate, created a simple on-paper pH sensor, demonstrated weight bearing, and showed separation of water from ultra-low surface tension hexane demonstrating the utility of our superomniphobic paper surfaces.

We also fabricated a smooth slippery copper surface by creating a chemically and physically homogenous surface. We developed a quick screening test to evaluate the performance of our surfaces in addition to the traditional tests. We showed smoother surfaces performed better and were more slippery.

ACKNOWLEDGEMENTS

I would like to express my special thanks and gratitude to Dr. Arun Kota who has given me the opportunity to do research and encouraged me to finish my work for my thesis in the field of Surface Science. I would like to thank Sanli Movafaghi and Wei Wang for all the support with the Scanning Electron Microscopy (SEM), scientific discussions, and trouble shooting support. I would also like to thank Breanna Novak for spending long hours in the lab performing tedious optimization. I would like to thank all students in Dr. Kota's research group: Hamed Vahabi, Lewis Boyd, Anudeep Pendurthi, Sranvanthi Vallabhunei, Dan Sutherland, and Prem Kantam for maintaining an active lab environment and engaging discussions during our research group meetings. I sincerely thank Dr. Travis Bailey and Dr. Ketul Popat for giving me their valuable time and feedback to improve this work and serve on my Masters committee. I would also like to thank the National Science Foundation (NSF) Louis Stokes Alliance for Minority Participation (LSAMP) Bridge to Doctorate (BD) Fellowship program for funding this work. I would also like to thank Dr. Gregory Florant and Dr. Mary Stromberger for all the help and support. Lastly, I would like to thank all those who supported my interest in research and graduate school including Aaron Benally, Trevor Aguirre, Dr. Scott Fulbright, Dr. Steve Albers, Dr. Ken Reardon, Dr. Troy Holland, Dr. Matt Kipper and all the other who have showed me continued support throughout my academic pursuits.

TABLE OF CONTENTS

CHAPTER 1: INTRODUCTION

Surfaces that display high lateral liquid droplet mobility are termed as “slippery”. These “slippery surfaces” are signified by very low contact angle hysteresis and very low sliding angles. Slippery surfaces have garnered interest due to their broad range of applications such as increased condensation heat-transfer, lab-on-chip devices, biomedical devices, etc.

Slippery Surfaces have different design criteria dependent on their surface topography or texture. As such, these surfaces can be broadly categorized into slippery non-textured surfaces and slippery textured surfaces. Non-textured surfaces are surfaces with low surface roughness, that are very smooth. Slippery non-textured surfaces allow droplets to easily slide laterally across the surface. These smooth surfaces can be made slippery by modifying the surface by imparting surface chemistry to make a very chemically and physically homogenous surface. Textured slippery surface do this via an air cushion created by super-repellant (superhydrophobic or superomniphobic) surface that gives high droplet mobility, causing liquid droplets to easily roll across the surface. These slippery textured surfaces will have appropriate texture, imparted with low solid surface chemistry and be super-repellant allowing a stable air layer between the liquid and the surface to form.

In this work we fabricated slippery textured surfaces and slippery non-textured surfaces. Our slippery textured surface was fabricated by growing nanofilaments on a glass microfiber paper and imparting low solid surface energy. Our slippery non-textured surface was fabricated by taking polished smooth copper and imparting chemical homogeneity via thiolation. In Chapter 2 we will cover the background and fundamentals of wettability, and define important properties used to design and evaluate a slippery surface. Chapter 3 will cover our textured slippery surface

and Chapter 4 will cover our smooth non-textured slippery surface. Future work and conclusions of our work will be included in Chapter 5.

CHAPTER 2: FUNDAMENTALS OF SURFACE WETTABILITY AND DESIGN OF SLIPPERY SURFACES

The wettability of a surface determines how a liquid wets the surface, and for the case for a small volume of liquid (droplet), it determines how much the liquid will spread on a solid surface. As shown in both nature and industry, surfaces can be tuned with different wettability to produce specific properties, such as corrosion resistance[1, 2] or trapping prey[3] (pitcher plant), for the desired application. Surface wettability is usually characterized by contact angle and contact angle hysteresis.[4, 5] These surfaces can have varying degrees of surface texture (smooth to rough). The texture will affect the design principles to make slippery surfaces. In this chapter, key concepts of surface wettability and design of slippery surfaces will be covered in detail.

2.1 Contact Angle (θ)

When a liquid droplet contacts a surface, the liquid will spread until it reaches an equilibrium. The angle between the tangents of the solid-liquid interface and the liquid-vapor interface at the point known as the triple phase contact line (i.e. the point where vapor-liquid-solid are in contact) is defined as the contact angle (Figure 1).

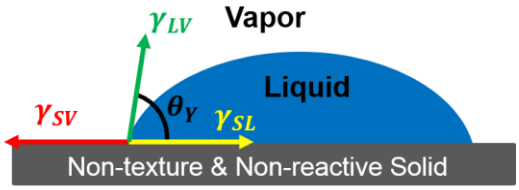

***Figure 1**: Schematic of both young's contact angle and the energy balance at the triple point for a liquid on a non-textured and non-reactive surface*

For non-reactive and non-textured surfaces, this angle is the thermodynamic equilibrium contact angle known as Young's contact angle (θ_Y). This is given by Young's relation:[6]

$$\cos\theta_Y = \frac{\gamma_{SV} - \gamma_{SL}}{\gamma_{LV}} \tag{1}$$

where γ_{SL} is the solid-liquid interfacial energy, γ_{SV} is the solid-vapor interfacial energy (solid surface energy), and γ_{LV} is the liquid-vapor interfacial energy (surface tension). This equation can be derived by considering a force balance at the equilibrium state at the triple-phase contact line as shown in Figure 1. As shown in Young's relation (Equation 1), generally lower solid surface energy or higher surface tension liquids lead to higher Young's contact angle. A surface with water contact angle greater than 90° is hydrophobic while a surface with water contact angle less than 90° is hydrophilic.

2.2 Contact Angle Hysteresis ($\Delta\theta$)

The second parameter typically characterizing surface wettability is the contact angle hysteresis ($\Delta\theta$). Contact angle hysteresis is defined as the difference between the advancing (θ_{adv}) and receding (θ_{rec}) contact angle of a moving droplet ($\Delta\theta = \theta_{adv} - \theta_{rec}$). The advancing contact angle is the maximum angle and the receding contact angle is the minimum contact angle displayed on the surface.

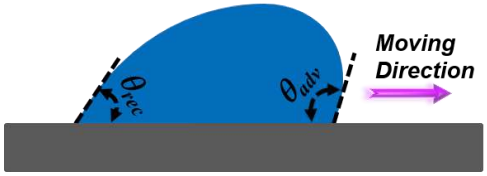

***Figure 2**: Schematic showing the advancing (forward) and receding (trailing) angles that develop as a droplet moves across a surface*

Physically, $\Delta\theta$ is a measure of the energy dissipated as a liquid droplet moves along a solid surface. As a droplet moves across the surface, the energy on the leading edge (moving direction) energy is released due to wetting the surface, and on the trailing edge work is expended as the droplet dewets the surface. At the leading edge, the moving droplet will display the maximum contact angle or the advancing contact angle, and at the trailing edge, it will display the minimum contact angled or the receding contact angle (Figure 2). In this work, we measured the advancing contact angle by taking the maximum measured angle when slowly increasing the volume (using a syringe) of a liquid droplet deposited on a surface. We measured the receding contact angle as the minimum contact angle of a droplet while reducing liquid volume slowly (using a syringe). A surface that has low contact angle hysteresis signifies a surface with high droplet mobility.

2.3 Textured Surfaces

As a liquid droplet contacts a textured surface, it displays an apparent contact angle (θ^*). This apparent contact angle is a property of both the texture and chemistry of the surface. It is also measured from the triple phase contact line (like Young's contact angle but now on a textured surface). To minimize its overall free energy, the droplet can adopt one of the following configurations after contacting the textured surface: the Cassie-Baxter[7] state or the fully wetted Wenzel[8] state. In the Wenzel State, a liquid fully permeates the surface protrusions (texture) to form a homogenous liquid-solid interface (Figure 3). A textured solid surface will have greater area than a perfectly flat smooth surface due to the surface roughness (textured). To characterize surface roughness, we can characterize the surface by a roughness factor (r):[8]

$$roughness\ factor\ (r) = \frac{actual\ surface\ area}{projected\ surface\ area} \tag{2}$$

The apparent contact angle in Wenzel can be determined by:[8]

$$\cos\theta_W^* = r\cos\theta_Y \tag{3}$$

where r is the roughness factor, θ_Y is Young's contact angle and θ_W^* is the apparent contact angle in the Wenzel State. Equation 3 shows that with an increase in roughness factor for the same surface chemistry, the contact angle displayed on a textured surface will cause an increase in contact angle on a hydrophobic surface (i.e. if $\theta_Y > 90°$ than $\theta_W^* >> 90°$) and a decrease in contact angle on a hydrophilic surface (i.e. if $\theta_Y < 90°$ than $\theta_W^* << 90°$).

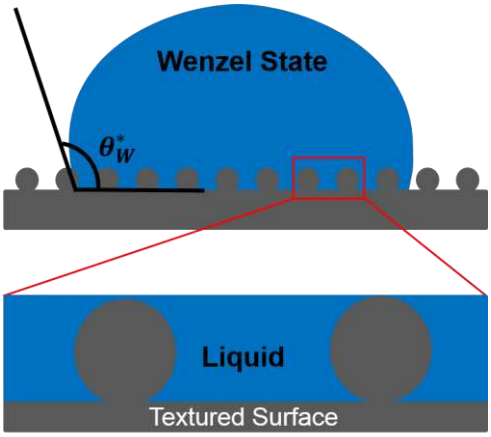

***Figure 3**: Textured surface with liquid in the Wenzel State (fully wetting the surface)*

Alternatively, in the Cassie-Baxter state, a liquid droplet that contacts a solid surface is not completely wet, and that air is trapped within the texture (Figure 4). The Cassie-Baxter apparent contact angle (θ_{CB}^*) on a surface can be expressed as:[7]

$$\cos\theta_{CB}^* = f_{SL}\cos\theta_Y + f_{LV}\cos\pi \tag{4}$$

where f_{LV} is the area fraction of the liquid and vapor interface and where f_{SL} is the area fraction of the solid-liquid interface. By increasing the liquid-vapor interfacial area, it is evident Equation 4 shows that the apparent contact angles will increase. On textured surfaces, the Cassie-Baxter

state is preferred to create a slippery surface as it helps prevent droplet pinning and create a lower contact angle hysteresis allowing easy lateral movement of the droplet.

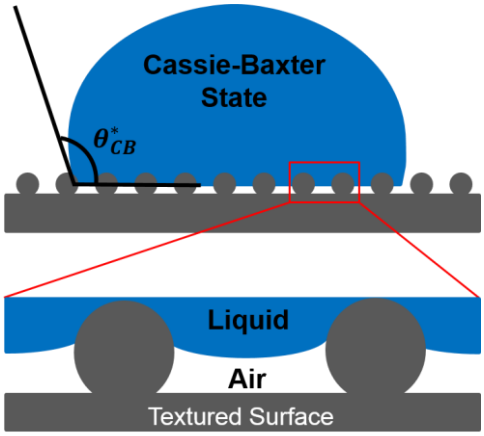

***Figure 4**: Textured Surface with a liquid in the Cassie-Baxter State*

2.4 Hierarchical Structure and Re-entrant Texture

While robust and stable Cassie-Baxter state can be achieved with most textures, not all textures can support a robust Cassie-Baxter state to low surface tension liquids.[5] Re-entrant textures are used to help achieve a stable Cassie-Baxter for both high surface tension liquids like water and low surface tension liquids like oils and alcohols. A surface texture is described as re-entrant if the vertical normal to the surface intersects the texture at two or more points. Figure 5 shows examples of texture that aren't re-entrant (Figure 5b) and of textures that are re-entrant

(Figure 5a).

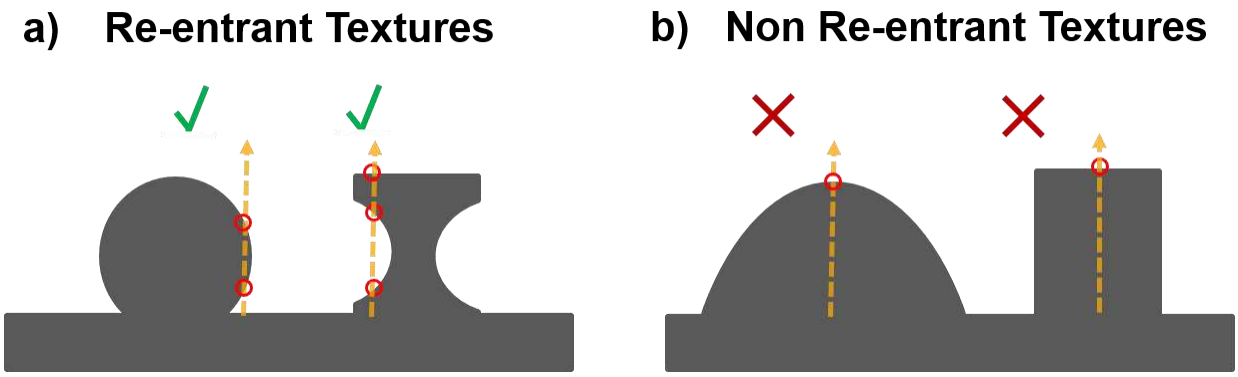

Figure 5: a) *Example of re-entrant textures as the normal intersects through at least two different points.* ***b)*** *Texture are no re-entrant as the normal only intersects through one point.*

Surfaces textured that have coarser length scale features that are covered with finer length scales are referred to as a hierarchical structure (Figure 6). A hierarchical texture in addition to the texture being re-entrant will further increase Cassie-Baxter stability than a re-entrant texture alone. Hierarchical structures where both length scales support the Cassie-Baxter state causes more air to be trapped, increasing the liquid-vapor (f_{LV}) area fraction making the surface display higher apparent contact angles (θ^*).[9]

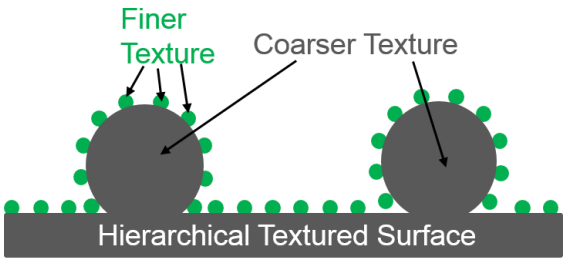

Figure 6*: Hierarchical textured surface with two length scales*

2.5 Roll-Off/Sliding Angle

Roll-off or sliding angle (ω) is the minimum tilt angle at which a liquid droplet sitting on a solid surface begins to slide or roll off from the surface (Figure 7). In general, slippery textured

surfaces cause droplets to roll, while slippery smooth surfaces cause droplets to slide. Slippery surfaces have low roll off angles for small volumes of liquids due to low lateral adhesion. As first shown by Furmridge, by performing an energy balance on by the work expended due to adhesion (right side Equation 5) and the work done by gravity (left side Equation 5), the roll off angle can be estimated from:[10]

$$\rho g V \sin\omega \approx \gamma_{LV} \, \mathrm{D}_{TCL} (\cos\theta^{*}_{rec} - \cos\theta^{*}_{adv}) \tag{5}$$

here, ρ is the density of the liquid droplet, g is the acceleration experienced due to gravity, V is the volume of the droplet, and D_{TCL} is the width of the solid-liquid-vapor contact line perpendicular to the rolling direction (this can be measured as the width of the droplet perpendicular to the sliding direct for sliding droplets show in Figure 7). Therefore, for a surface tilted at an angle α relative to the horizontal, the liquid droplet will roll or slide if the tilt angle is greater than or equal to the roll off angle ($\omega \leq \alpha$).

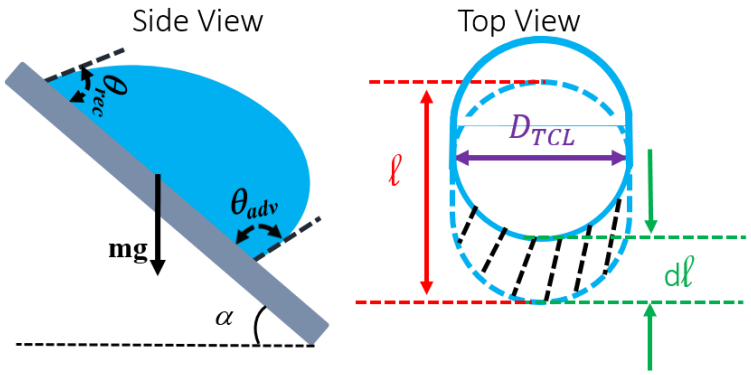

***Figure 7**: Liquid droplet sliding on a surface tilted at angle α*

2.6 Design of Textured Slippery Surface: Superhydrophobic vs Superomniphobic

Slippery textured surfaces will maintain Cassie-Baxter state to easily allow a droplet to roll across its surface. The surfaces are super-repellant to liquids and are broadly categorized as either being superhydrophobic or superomniphobic. A surface that is superhydrophobic will have

high apparent contact angles for water and other high surface tension liquids ($\theta^* \geq 150°$). A superomniphobic surface will display high apparent contact angles for both high surface tension and low surface tension liquids. To create a slippery superomniphobic or superhydrophobic, the surface must maintain a stable Cassie-Baxter state to prevent partial or full Wenzel state, which causes pinning, as not all superomniphobic/superhydrophobic surfaces are slippery.[11, 12] Using appropriate hierarchical and re-entrant texture with uniform low solid surface energy surface, we can create a slippery textured superomniphobic surface.

2.6 Design of Non-textured (Smooth) Slippery Surfaces

Contact angle hysteresis arises from surface roughness and heterogeneity.[13, 14] Non-textured slippery surfaces must be very smooth and homogenous to give a surface low contact angle hysteresis. To quantify the smoothness of the surface, the root mean square roughness (R_{rms}) was used. This is the root mean square average of the deviations of the profile from the mean line and gives a relative idea of the smoothness of the surface. This can be measured using atomic force microscopy (AFM) or optical profilometry, which were used in this work. Surfaces that are very physically smooth and very chemical homogenous will be very slippery. In this work, we polished copper and modified its surface to give it the necessary physical and chemical homogeneity to make it slippery.

CHAPTER 3: FABRICATION OF SUPEROMNIPHOBIC PAPER: A TEXTURED SLIPPERY SURFACE

Super-repellant textured surfaces (surfaces that display high apparent contact angles i.e. $\theta^* \geq 150°$) are generally categorized as either superhydrophobic (i.e. surfaces that are extremely repellent to high surface tension liquids such as water $\gamma_{LV} = 72.1$ mN m^{-1}) or superomniphobic (i.e. surfaces that are extremely repellent to both high surface tension liquids like water and low surface tension liquids like oils such as hexadecane $\gamma_{LV} = 27.5$ mN m^{-1}).[1, 2, 5, 15-22] As these surfaces have numerous real-world applications, they have been fabricated on an array of numerous material substrates such as steel[19, 20], polymers[2], copper[23, 24], silicon[25, 26] , or paper[18, 27-29]. In particular, paper substrates have garnered interest due to paper's properties such as flexibility, low-cost, light weight, and renewability. While there have been numerous reports of superhydrophobic papers[30-36] in the literature with droplet mobility, there have been virtually no reports, except one prior report[37], of using paper's texture to create a slippery superomniphobic paper surface with high droplet mobility (i.e. paper surface with low roll off angle and high contact angle for low surface tension liquids). In this work, we first created a re-entrant textured and hierarchically structured paper surface by growing silicone nanofilaments (finer texture) on glass microfiber paper (native coarser texture). We then imparted low surface energy via vapor phase silanization with a low surface energy silane. The final paper surface was superomniphobic with high droplet mobility demonstrated by having roll-off angle $\omega < 10°$ for both a low surface tension liquid (e.g., hexadecane) and a high surface tension liquid (e.g., water). Taking advantage of our superomniphobic paper surface, we demonstrate several

potential applications such as pH sensor, weight bearing, high droplet transport rate, anti-corrosion resistance and water-hexane separation.

3.1 Materials and Methods of Fabrication for Superomniphobic Paper Surface

To create a superomniphobic paper surface, we needed to create a hierarchically structured surface and impart a low solid surface energy (γ_{SV} < 15 mN m^{-1}). To do this, we used a method to grow silicone nanofilaments[25, 38], which we performed on our glass microfiber paper surface (VWR glass fiber filters grade 691). In atmospheric conditions, 20 ml of toluene was mixed with 1 μL deionized (DI) water which was shaken gently for 2 minutes, followed by addition of 400 μL of trichlormethylsilane (TCMS), which was shaken gently for 5 minutes prior to paper immersion in the solution. Prior to growing nanofilaments, glass microfiber paper was first cleaned by sonication in acetone and then ethanol, each for 5 minutes followed by drying with nitrogen. Samples were treated with O_2 plasma for 15 minutes and exposed to water vapor from a humidifier for 30 seconds to activate the surface. Immediately after water vapor exposure of the microfiber paper, the samples were immersed into the solution of DI water, toluene and TCMS. The paper was kept immersed in the solution and placed in a controlled humidity chamber. We kept the chamber humid (>60% relative humidity) using a constant stream of water vapor from the humidifier and left this whole system idle for 4 hours. After treatment, samples were annealed on a hot plate for 2 hours at 200 °C. Following annealing, samples were rinsed with toluene, ethanol, 50% v/v DI water/ethanol successively, followed by drying with nitrogen. At this point the samples displayed superhydrophobicity due to the chemistry of the TCMS nanofilaments, but not superomniphobicity (oils would stick and spread on the surface). We next imparted low solid surface energy ($\gamma_{SV} \approx$ 10 mN m^{-1}) on the surface by activating the surface for

15 minutes via O_2 plasma followed by vapor phase silanization with heptadecafluoro-1,1,2,2-hydrodecyltrichlorosilane (FDTS) from Gelest. The vapor phase silanization was performed on a hot plate for 1 hour at 120 C˚ using 200 µL of FDTS in a closed system. It is important to note that as received microfiber paper samples that were vapor phase silanized (imparted with low surface energy) only displayed superhydrophobicity, and did not have high droplet mobility for low surface tension liquids like oils showing the necessity of the hierarchical structure formed from the nanofilaments.

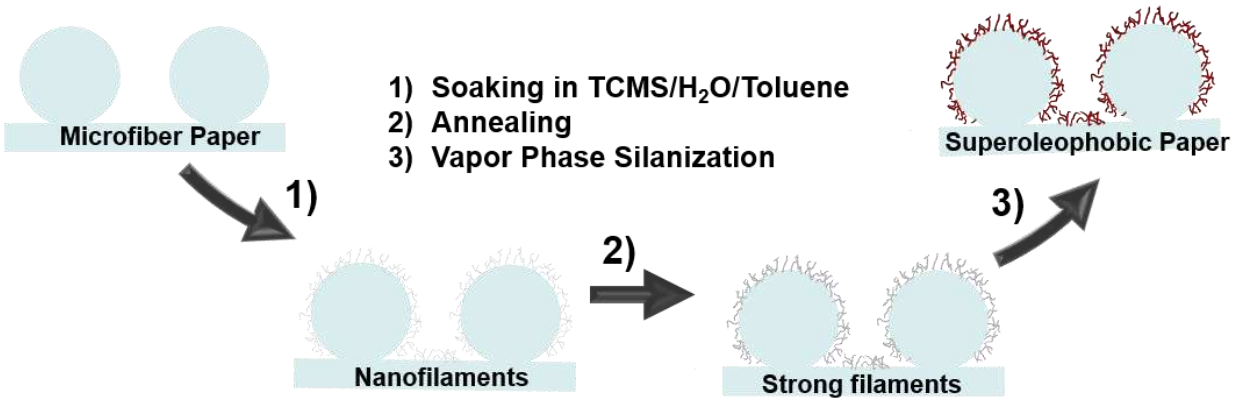

Figure 8:*Fabrication Process of Superomniphobic Paper Surfaces*

The first step created superhydrophobic nanofilaments and the final step made the surface superomniphobic and highly slippery to both low and high surface tension liquids. Final samples of our superomniphobic paper surface showed high apparent contact angles for both low surface tension hexadecane (dyed red) and high surface tension water (dyed blue) in Figure 9.

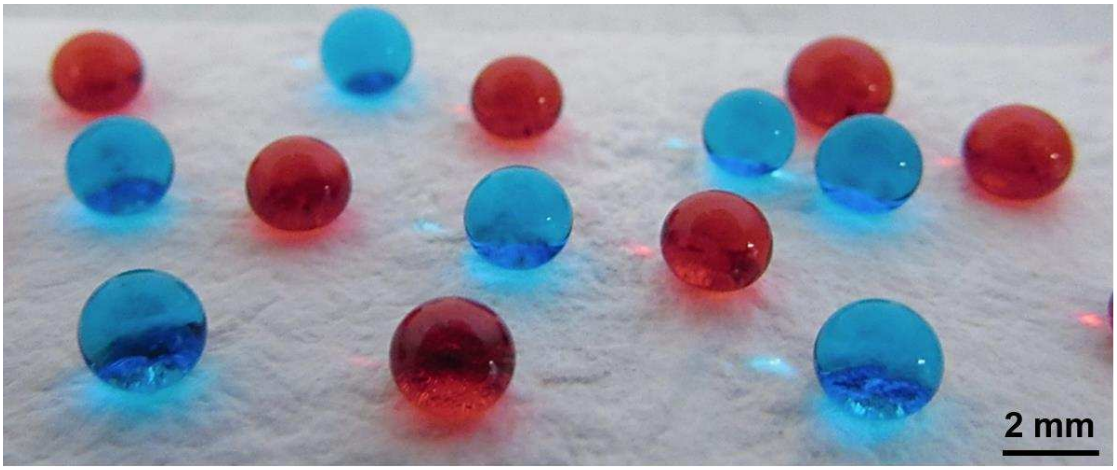

Figure 9: *Super-repellancy of both hexadecane (red; 27.1 mN m^{-1}) and water (blue, 72.1 mN m^{-1})*

3.3 Characterization and Performance of Superomniphobic Paper Surfaces

Properties such as roll-off angle, surface morphology, contact angle and contact angle hysteresis of superomniphobic paper were characterized. Surfaces were imaged with a scanning electron microscope (SEM) (JEOL JSM-6500F) at 15 kV to determine the surface morphology. Images show the as received samples and samples with the grown nanofilaments in Figure 10, at different length scales. The paper surfaces had microfibers with diameters of ~ 0.5-2.5 µm and the nanofilaments had diameters of ~ 40-100 nm. The SEM images show the hierarchical structure of the superomniphobic paper surface in Figure 10.

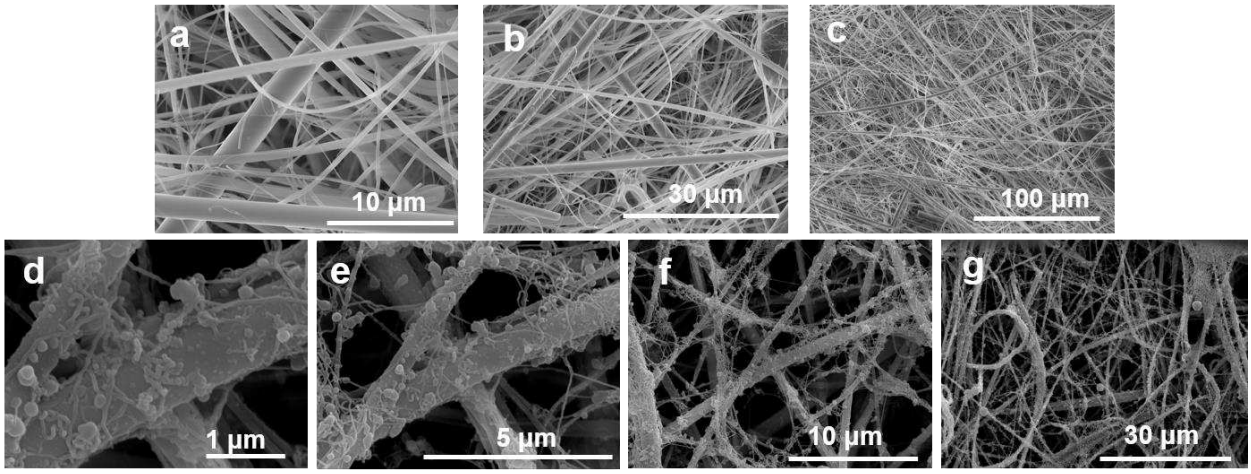

***Figure 10**: **a-c)** Shows images of as received paper before modification. **d-g)** Shows images of final superomniphobic paper surface.*

To characterize the surface wettability, we measured advancing (θ^*_{adv}), receding(θ^*_{rec}), and roll-off angles (ω) with liquids of different surface tensions. These measurements were done using a Rame'-Hart 260-F4 goniometer. We measured contact angles using ~8 µl droplet. Roll-off angle was measured by placing an 8 µl droplet on the surface, then slowly tilting the surface until the droplet begins to roll. The angle the droplet first began to roll was recorded as the roll-off angle. To gather data from liquids with different surface tensions, we used hexadecane, water, dimethylformamide and mixtures of water with varying SDS concentrations (1 mM, 2 mM, 3 mM, and 5 mM). The data shows (Figure 11) that these surfaces are superomniphobic as they display high apparent contact angles (θ^* > 150°) for low and high surface tension liquids and are slippery as they display the desired high droplet mobility (ω < 10°) for the liquids.

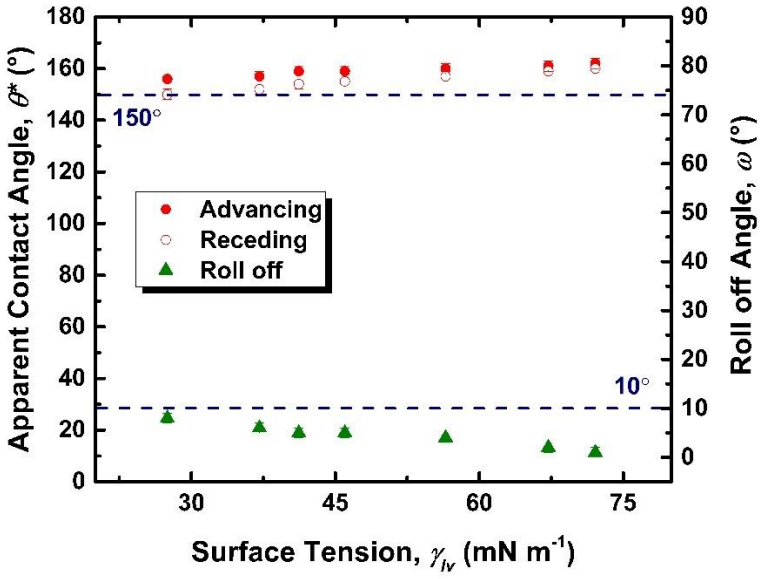

Figure 11: *Shows advancing, receding and roll-off angles from liquids of different surface tensions on the superomniphobic paper surface. Left to right hexadecane(27.5 mN m^{-1}), dimethylformamide(37.1 mN m^{-1}), 5 mM SDS(41.2 mN m^{-1}), 3 mM SDS(46.0 mN m^{-1}), 2 mM SDS(56.5 mN m^{-1}), 1 mM SDS(67.2 mN m^{-1}), and water(72.1 mN m^{-1})*

The roll-off angle measured follows the trend for the predicted roll-off angles from Furmidge equation (see equation 5), based on the contact angle measurements and liquid properties. All measurements were performed intrasample with the error recorded as the standard deviation or the measurement error (whichever was larger). All tested liquids displayed the desired performance of $\theta^* > 150°$ and for $\omega < 10°$. The graph shows the trend that apparent contact angles decrease with decreasing surface tension. This trend is statistically significant (see Appendix A), as water and hexadecane are shown to be different. The trend that rolling angle decreases with decreasing surface tension is supported as rolling angle data points between points at least two apart (~ 20 mN m^{-1}) were statistically different. Figure 11 shows our superomniphobic paper surface to be slippery, indicated by the low roll off angles, for both low and high surface tension liquids.

3.4 Chemical Resistance

To create a pH sensor, our superomniphobic paper surface must be chemically resistant to corrosive liquids (i.e., acidic and basic liquids), as many previous super repellant surfaces have shown. [2, 17] To test the chemical resistance to corrosive liquids, we submerged our superomniphobic surfaces in a range of liquids of different pHs for one hour. Solutions with different pHs were prepared using hydrochloric acid or sodium hydroxide. Our superomniphobic paper surfaces retained their properties and showed little change in performance after immersion in these corrosive solutions for 1 hour (i.e., little change in roll-off angle of water).

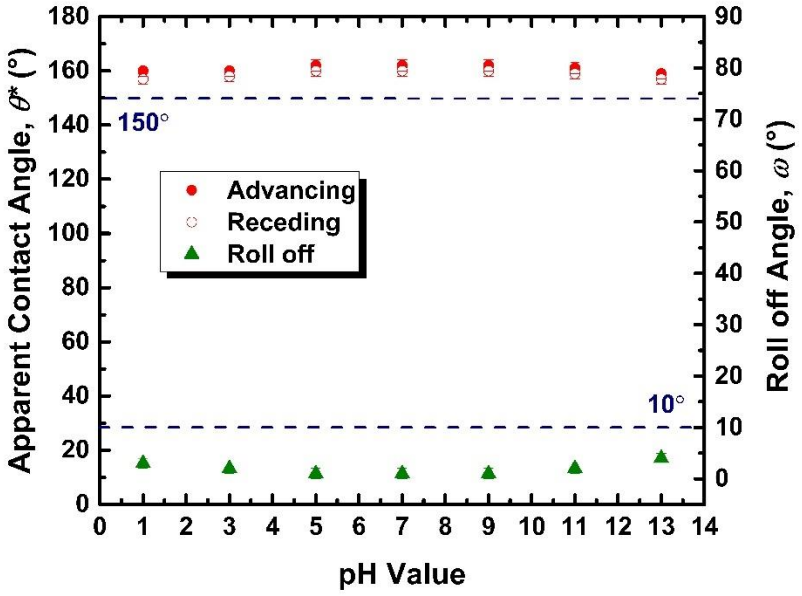

Figure 12: *Immersion of superomniphobic paper into solutions of varying pH yielded no change in performance. Measurements were done with water.*

Advancing (θ^*_{adv}) and receding (θ^*_{rec}) apparent contact angles showed no statistically significant difference after exposure for one hour to any of the pH values tested, as shown in Figure 12. The roll-off angle (ω) showed no statistically significant difference after exposure in the range from pH 3 to pH 11. There was a statistically significant change in performance after surface exposure

to pH 1 or pH 13, but the performance changed very little, indicating the surface is still slippery enough for practical use. Even though there was a definite change to roll-off performance at the extremes, the change was very small allowing for the necessary and consistent performance for pH values necessary to create a pH sensor.

3.5 High Droplet Transport Rate for On-Paper Systems

Droplet or liquid transport rate is important for point of care or lab-on-chip devices to be quick to use. To demonstrate this possibility, we first demonstrated guided droplet transport on our surface. We first created a guiding rail by drawing a straight line with a No.2 pencil on our superomniphobic paper surface. This graphite line created a wettability contrast between the line and the surrounding surface and allowed the droplet to be guided down the along the straight line when tilted. In comparison to in-paper point-of-care microfluidic devices, when we tilted our surface, our droplet showed exceptionally fast transport rate (~ 12 cm/s) for long distances and no liquid loss on the guiding rail, as shown in Figure 12.

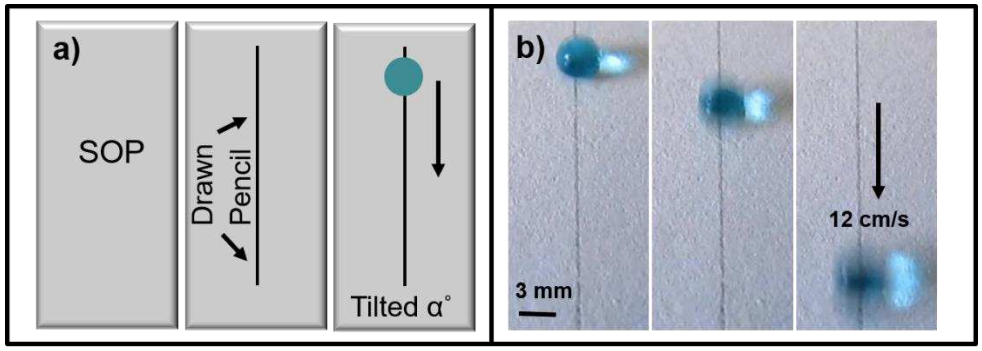

Figure 13: a) *Schematic of guiding rail.* ***b)*** *Fast droplet transport at tilted angle α = 20°.*

3.6 pH sensor and sensor fabrication

We fabricated a simple pH sensor taking advantage of these properties to demonstrate a potential lab-on-paper type device. To fabricate a pH sensor using our superomniphobic paper

surface, we first created three domains on the paper surface using the No. 2 pencil. Next, between each domain we placed a graphite guiding rail. In each domain, we deposited three different pH indicators (M-Nitrophenol, Phenolphthalein, Thymolphthalein). We can use each domain to test the pH of the droplet, a schematic of the design is shown in Figure 13.

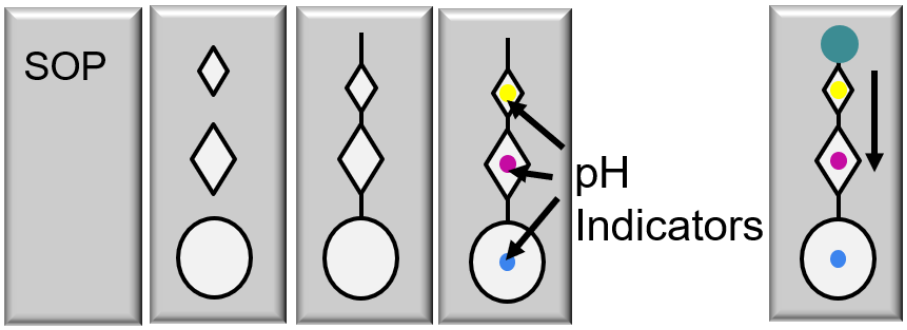

Figure 14: *Shows schematic of steps to fabrication on-paper pH sensor*

To trap the droplets of the pH indicators into the domains, we had to change the wettability in each domain to increase wettability. Paraffin wax was dissolved in chloroform and subsequently deposited into each domain. After deposition of the wax, the pH indicators can be deposited into the domain. The pH indicators were prepared the following way with the following properties: M-Nitrophenol 2.125 mg per ml (colorless to yellow pH > 6.8) in 37.5 % volume ethanol in water with 0.3 µL of the final mixture deposited into domain 1. Phenolphthalein 0.8 mg per ml (colorless to pink/fuchsia pH > 8.2) in 50 % volume ethanol was mixed into ethanol in water with 0.3 µL final mixture deposited into domain 2. Thymolphthalein 0.83 mg per ml (colorless to blue pH > 10.5) was mixed into a 75 % volume ethanol in water with 2 µl of the final solution deposited into the last domain, domain 3.

To use the pH sensor, a droplet (~8 µL) was first set on the guiding rails above the first domain. The droplet would roll and stop in the first domain due to the increased wettability and adhesion. The droplet would react quickly and indicate the appropriate color change based on the pH of the droplet. For a droplet to leave any domain, the kinetic energy must be greater than the

adhesion energy of the domain. To get the droplet to leave the first domain, we dropped a second droplet of the same liquid (~8 µL) to give the droplet the necessary energy from the collision kinetic energy. The now rolling droplet (~16 µL), on the guiding rail, did not have the necessary velocity (kinetic energy) to pass the second domain. Since the adhesion energy of the second domain was more than the kinetic energy of the droplet, the droplet stopped in the second domain allowing it to react with the indicator. This process is repeated so that the droplet can move from the second domain to stop in the final domain. This process is shown in Figure 15.

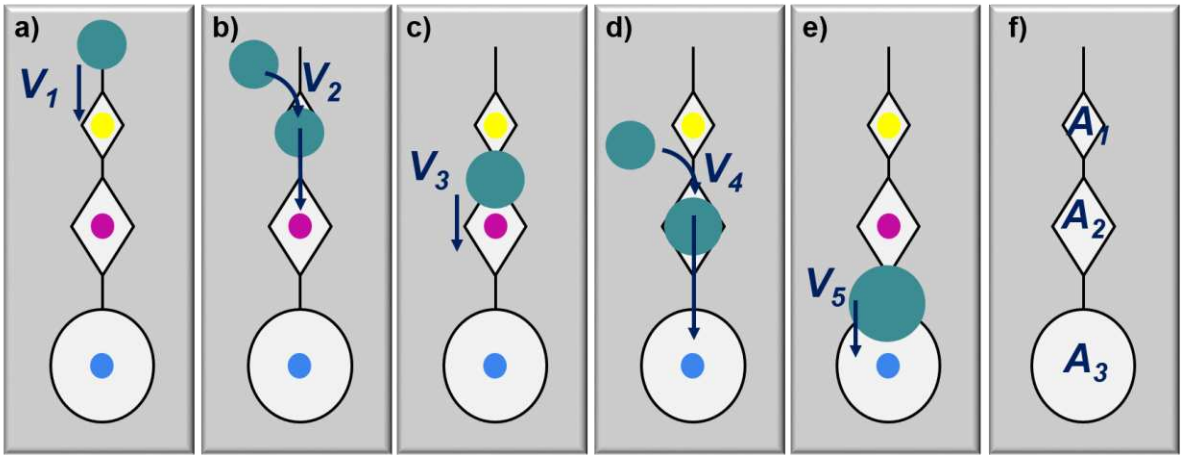

Figure 15: a-e) *Shows the process for using the pH sensor and labels the velocities to be used in energy estimation.* ***f)*** *Showing A_1, A_2, A_3 are the labels area for each specific domain.*

For the droplet to leave each domain and adhere to the next domain the following inequalities based on an energy balance (adhesion energy vs. kinetic energy) must be true. Each inequality (a-e) matches the step shown in Figure 15.

a) $$\frac{1}{2}mv_1^2 \leq \gamma_{LV}(\cos\theta^*_{rec,wax} - \cos\theta^*_{adv,graphite}) * A_1$$

b) $$\frac{1}{2}mv_2^2 > \gamma_{LV}(\cos\theta^*_{rec,wax} - \cos\theta^*_{adv,graphite}) * A_1$$

c) $$\frac{1}{2}(2m)v_3^2 \leq \gamma_{LV}(\cos\theta^*_{rec,wax} - \cos\theta^*_{adv,graphite}) * A_2$$

d) $\frac{1}{2}mv_4^2 > \gamma_{LV}(\cos\theta^*_{rec,wax} - \cos\theta^*_{adv,graphite}) * A_2$

e) $\frac{1}{2}(3m)v_5^2 \leq \gamma_{LV}(\cos\theta^*_{rec,wax} - \cos\theta^*_{adv,graphite}) * A_3$

Where the $v\#$ is the velocity corresponding to the droplet shown in Figure 15, m is the mass of the droplet (with a volume of 8 µL for our experiment), $\cos\theta^*_{rec,wax}$ is the receding angle on the wax, $\cos\theta^*_{adv,graphite}$ is the advancing angle on the No. 2 pencil, and (A_1, A_2, A_3) are the corresponding domain areas based on the schematic in Figure 15.

Based on the quality of the video showing the pH sensor, we were unable to accurately estimate several of the velocities for v_1, v_2, v_5 while the other velocities were very rough estimations due to the relatively low framerate on the camera. The calculations work out if we make two additional assumptions based on things known from the experiment. One, if we assume as the droplets left domain 1 and domain 2 that the potential energy of the droplets dropped into the sitting droplet (Figure 15 b,e) was equal to the kinetic energy of the droplet (i.e. we assume $\frac{1}{2}mv_4^2 \approx mgh$ and $\frac{1}{2}mv_2^2 \approx mgh$ where (h) is the height the droplet is dropped from and (g) is gravity). Second, if we assume v_1 was small as the droplet was gently set at the top of the sensor, as was done in the experiment, the rough calculations work and fit the listed inequalities.

We demonstrated the ability to detect a range of pHs with this system, as shown in Figure 16. This functionality demonstrated the ability to the development of lab-on-paper type devices using our superomniphobic paper surface. For example, our already simple system can be

changed such that each domain can be used to host protein sensors or other chemical reagents to test liquids using a small volume (in this case 24 µl total) in the form of liquid droplets.

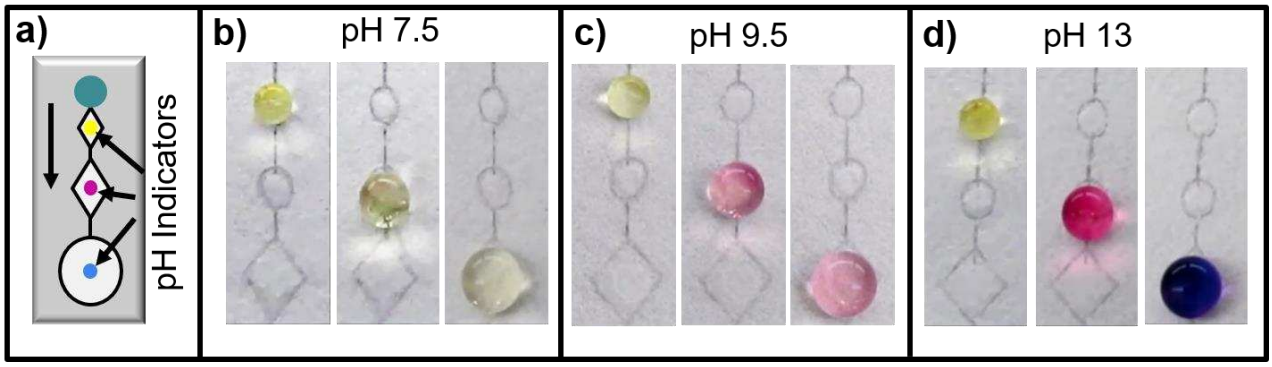

Figure 16: a) *Design of pH sensor.* ***b-d)*** *Demonstrating pH sensor by testing different aqueous solutions with a range of pHs (7.5, 9.5 and 13).*

3.7 Weight Bearing Capabilities

Recent work[2] has shown that flexible substrates can lead to higher weight bearing capabilities compared to their inflexible counterparts of similar thickness and lateral dimensions. Due to superomniphobicity, our surfaces can be used for weight bearing in a wide range of high and low surface tension or corrosive (i.e. acidic or basic) liquids. The weight bearing capacity is the maximum weight that a sample can support while floating (before sinking). We measured the weight bearing capacity of superomniphobic paper surfaces with ~0.9 cm diameter. The paper had weight bearing capacity of 47 mN and 34 mN on water and rapeseed oil, respectively, as shown in Figure 17.

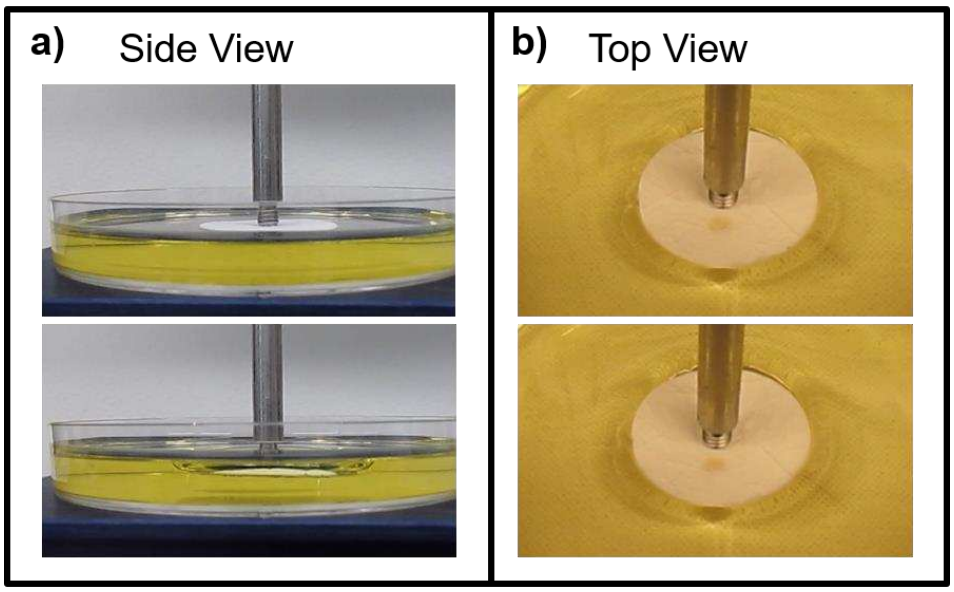

Figure 17: *Showing weight bearing capacity on rapeseed oil.*

3.8 Water-Oil Separation

Our superomniphobic paper surface repels a wide range of liquids with surface tensions ($\gamma_{LV} \geq 21$ mN m^{-1}), but ultra-low surface tension liquids like hexane (γ_{LV} = 18 mN m^{-1}) were readily wetted the surface on contact. This wetting of ultra-low surface tension liquids allowed us to perform a separation. We demonstrated this by performing a gravity separation of water and hexane, as shown in Figure 18.

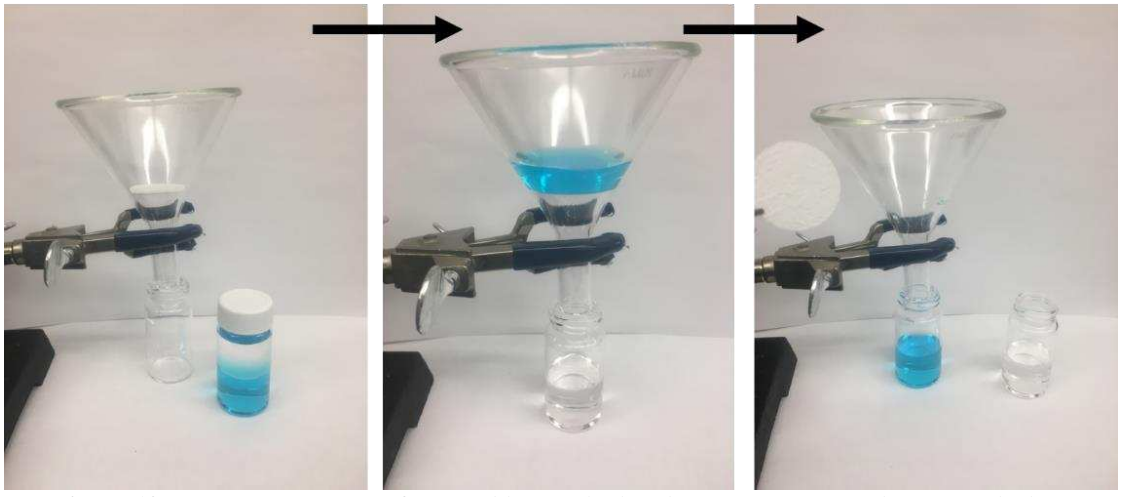

Figure 18: *Gravity separation* of *water (blue) with ultra-low surface tension hexane (colorless)*

Hexane passed through the membrane pores while water was unable to. The water was unable to pass through the paper either when the filter started dry or after the hexane had passed through. After the hexane passed through, some of the hexane stayed lodged into the membrane leaving the membrane wet creating a lubricated type surface. This wet membrane did not allow water to pass through. Even after letting the membrane completely dry, water would not pass through, showing the ability to re-use paper substrates for separation.

CHAPTER 4: FABRICATION OF NON-TEXTURED SMOOTH SLIPPERY COPPER

Non-textured slippery surfaces allow droplets to easily move across their surfaces due to low lateral adhesion. These surfaces have low contact angle hysteresis created by first being very physically smooth and homogenous, and second being chemically homogenous with appropriate chemistry.[39, 40] A number of smooth slippery surfaces have been made primarily on glass and silicon wafer substrates using an array of different chemistries.

Making a slippery copper surface has a lot of appeal due to copper being commonly used for many industrial application such as condensation heat transfer.[23, 41] As such, textured slippery superhydrophobic copper surfaces have been made using an array of different methods. There are multiple reports of low contact angle hysteresis copper surfaces[42, 43], but the slipperiness of these surfaces has not been explored.

During conventional condensation heat transfer, a cool surface comes into contact with hot vapor. As the vapor comes into contact with the surface, water vapor will begin to nucleate and condense onto the surface. As the droplets continue to grow and coalesce, a film will eventually form, resulting in filmwise condensation with a lower heat transfer coefficient. If a surface is covered in a promoter, but more specifically, if a surface is slippery enough, droplets will slide off and get removed from the surface, resulting in dropwise condensation with much higher heat transfer coefficient.

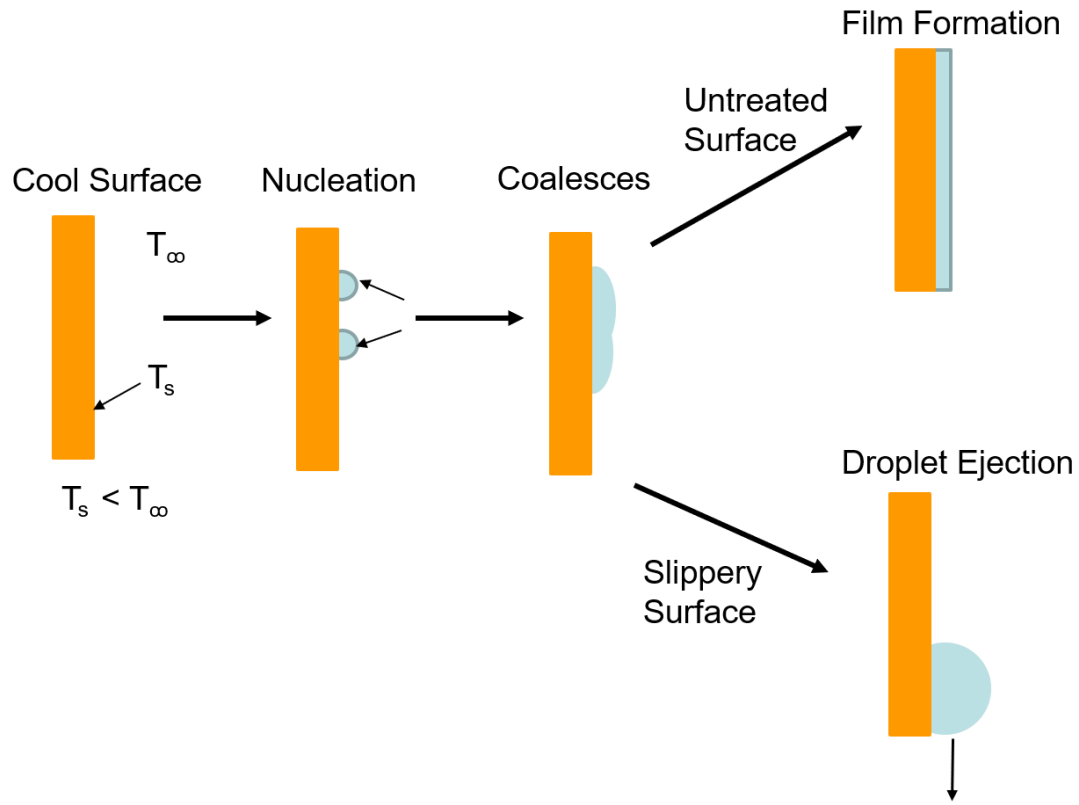

Figure 19: *Shows condensation heat transfer. Droplet ejection during dropwise condensation heat transfer increases heat transfer.*

To enhance dropwise condensation, typically promoters[44] have been used. Further, textured copper coatings or thick chemical coatings that would increase condensation heat transfer have been explored.[23, 41, 45] In this work, we fabricated a non-textured slippery copper surface and quantified its slipperiness. Our procedure, developed to create a chemically and homogenously smooth copper surface, could be used to enhance dropwise condensation.

4.1 Fabrication of Smooth Slippery Copper Surface

Copper plates with a mirror finish (on one side) were purchased from McMaster (SKU 9821K13). Pieces were cut for testing with a bench cutter. Samples were cleaned through sonication in acetone, followed by sonication in 70 % ethanol, each step for 5 minutes. Oxidized

copper is known to increase surface roughness and affect thiolation.[46, 47] To remove the oxidized layer to improve thiolation, the copper was first dipped and gently stirred in an acid solution for 30 seconds. A 100 mM dodecanethiol solution was prepared and nitrogen bubbled for 1 minute. Liquid dodecanethiol (Acros Organics CAS 112-55-0) was added and gently mixed into DI water to the desired concentration to create the thiol solution. Copper samples were placed into the thiol solution for 1 hour. Samples were removed after one hour and rinsed thoroughly with DI water, toluene, isopropanol, and again with DI water. Samples were dried with nitrogen before testing.

The thiolated copper plates were tested on both the side with the mirror finish and the non-finished side after thiolation. The mirror finish side had much lower roll-off angles for water droplets, likely due to more uniform physical and chemical homogeneity. Due to this, a polishing procedure was developed for copper to be able to create a more slippery surface that can potentially enhance dropwise condensation.

The following polishing procedure was developed and used to polish copper samples. For small sample sizes, the copper would be adhered to a polishing tool using crystal bond to stick to the tool. If the sample is not pre-polished on one side, both sides need to be polished simultaneously to ensure that the sample is sitting evenly on the tool to lead to a uniform polish. The polishing wheel was set to 250 rpm and polished wet (using water) on 240, 320, 600, 800, and 1200 grit sandpapers (Pace Technologies). At each step, the surface was polished until the surface appeared uniform. Subsequently, the surface was gently cleaned with a badger hair brush and soapy water, followed by rinsing with water, isopropanol and finally drying with a heat gun. After the grit paper, a pad with 1 micron polycrystalline suspension and dialube extender was used to polish the sample until a uniform mirror finish was obtained (roughly 20 – 30 minutes).

Samples were gently cleaned before the final step. A 0.05 micron alumina powder was smeared onto a pad using a water drip until the powder was a paste. The polishing wheel was set to 50 rpm and samples polished for 30 to 45 minutes creating more paste as needed to finish the polish. Samples were cleaned and inspected for uniformity in the last step by gently rinsing with water and cleaning with a fresh cotton ball. After polishing, samples were rinsed with water, isopropanol, and dried with a heat gun. Final samples were thiolated before testing.

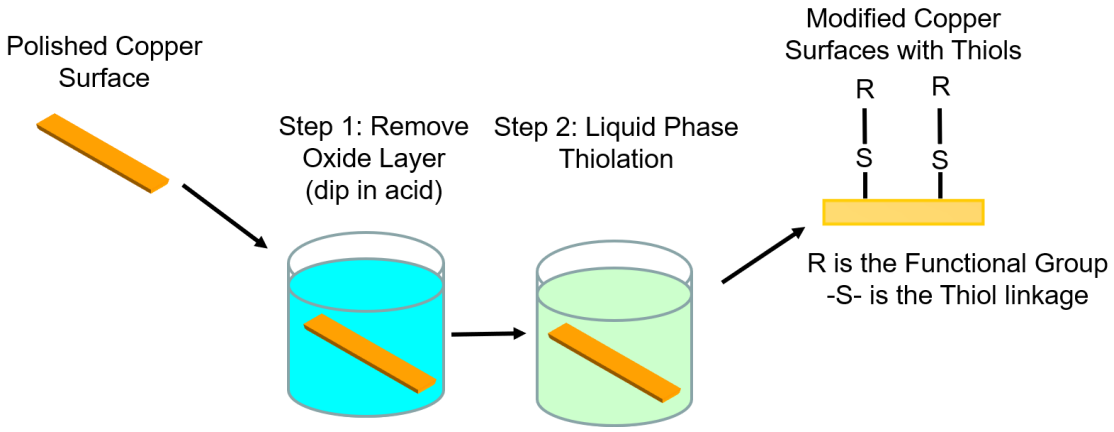

Figure 20: *Sows fabrication steps for making slippery copper surfaces*

4.2 Characterization and Performance of Smooth Slippery Copper Surfaces

Optical profilometry was used to characterize the root mean square roughness (R_{rms}). Roughness measurements were taken on a copper block, a polished copper block, the stock copper plate, and the mirror finish side of the stock copper plate. Measurements were also taken after thiolation on the two smoother surfaces, which were thiolated following the previous specifications.

Table 1: *Surface roughness (R_{rms}) of copper from optical profilometry*

Sample	R_{rms} [nm]
Copper Block	332 ± 120
Polished Copper Block	13 ± 2
Thiolated Polished Block	27 ± 7
Copper Plate	140 ± 13
Copper Plate Mirror Finish	34 ± 2
Thiolated Copper Plate Mirror Finish	45 ± 7

There was statistically significant difference between as received samples, polished samples, and the thiolated surface. Thiolating the surface increased surface roughness slightly. The polishing process can be used on either a block or copper plate to make it smoother before thiolating.

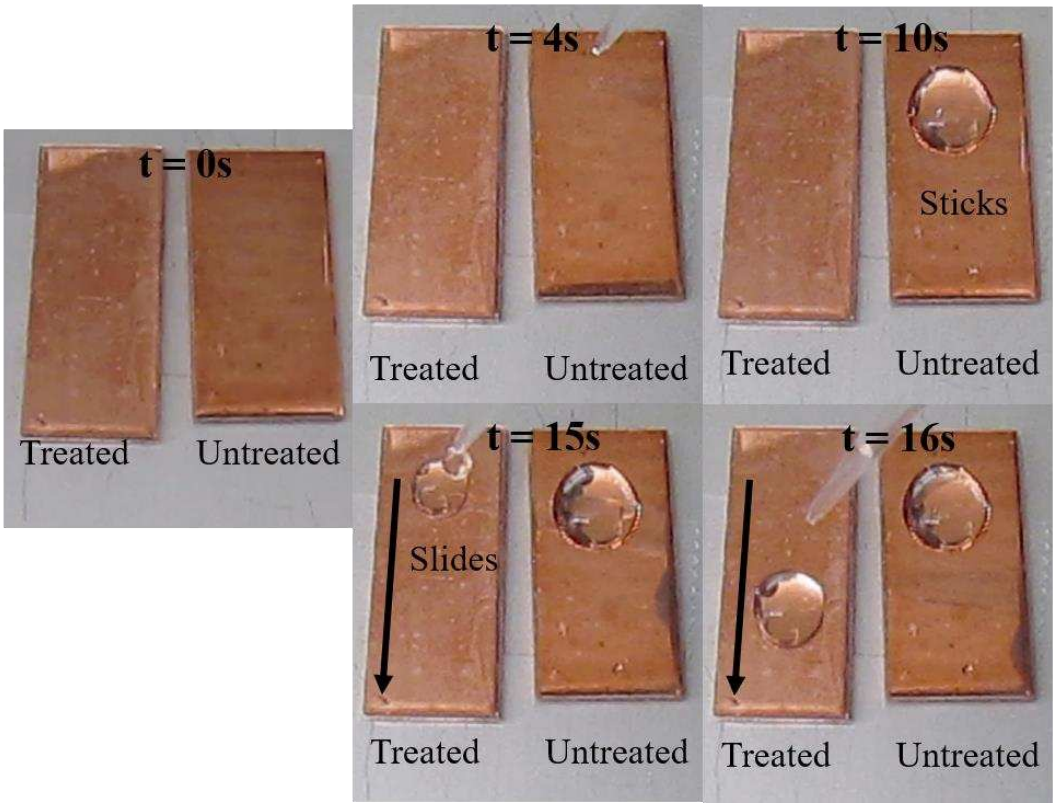

Figure 21: *Shows a 40 µL droplet sliding on a treated surface when tilted and sticking to an untreated surface.*

Treated surfaces showed visibly increased slipperiness compared to non-treated surfaces. Water droplets would stick to the as received copper but would slide on the thiolated surfaces. To measure performance and slipperiness of the thiolated surfaces, two measurements were used. The first was sliding angle on the copper surfaces, and a second was developed based on the potential application of enhanced heat transfer condensation. The second test, referred to as a 90˚ test, measured the smallest liquid water droplet volume that would slide on the surface when the surface was slowly tilted to 90˚. To perform this test a small volume of water was deposited on the treated surface, the surface was gently and quickly tilted to 90 ˚. If the droplet slid, the test would be repeated with a smaller volume of water. If the droplet did not slide, the volume of water would be increased and the test repeated. The recorded values are the smallest volume of water that would slide repeatedly if the test was performed again.

Copper will rapidly oxidize in the presence of air. This increases roughness of the surface and can interfere in thiolation of the surface.[43, 46, 47] Gold, a surface that also undergoes thiolation, does not oxidize. Sputtering pure gold onto different surfaces will give an idea of how much the oxidation or surface roughness is reducing the performance. Sputtering gold on the copper plate mirror finish appeared to slightly reduce R_{rms} [nm] of the surfaces to 28 ± 7 compared to 34 ± 2 before sputtering.

Table 2: *Shows performance of optimized samples*

Thiolated Surface	Sliding angle (°) (for 60 µL droplets)	90° Test (µl)
Copper Plate	>40	>10
Copper Plate Mirror Finish	12 ± 5	7 ± 1
Copper Mirror with Sputtered Gold	9 ± 3	4 ± 1
Silicon Wafer Sputtered Gold	6 ± 2	2 ± 1

Silicon wafers are extremely smooth, often with reported $R_{rms} \leq 1$ nm.[48] Here, we see the smoother surfaces outperformed the rougher treated surfaces. The values in the table are statistically different, suggesting that smoother surfaces perform better.

CHAPTER 5: CONCLUSIONS AND FUTURE WORK

5.1 Conclusions

In this work, we have fabricated two different slippery surfaces. The first slippery surface, a slippery textured superomniphobic paper surface, was fabricated by creating a hierarchically textured surface and imparting low surface energy. Our surface demonstrated high droplet transport rate and chemical resistance. This allowed us to make a simple lab-on-chip style device by fabricating a pH sensor using our slippery superomniphobic paper surface. We also demonstrated other potential applications such as weight bearing and separation of water and ultra-low surface tension oil.

Our second slippery surface is a non-textured smooth slippery copper surface. We were able to make a physically and chemically smooth surface with high droplet mobility on copper. To fabricate our surfaces, we dipped a polished copper surface into acid, then thiolated the surface. We used a 90˚ test and sliding angle to quantify the performance. The characterization showed great improvement in slipperiness of copper.

5.2 Future Work

In this work, we developed a pH sensor using our superomniphobic paper surface to demonstrate a lab-on-chip application. Future work should include finding and testing other potential lab-on-chip uses using the superomniphobic paper. Developing potential methods for streamlining or speeding up the fabrication process will greatly increase utility of our surfaces. Data analysis was performed using intra-sample data sets due to long fabrication times and inter sample variability due to condition variability. A streamlined and optimized system of

fabrication with better humidity control will allow for faster fabrication and inter sample variability analysis. The surface coverage from the silanization can be further analyzed, quantified and optimized by using X-ray Photoelectron (XPS) spectroscopy. Further, chemical resistance was shown with no significant change for most pHs, to a very small change at pH 1 and pH 13. It is not known if longer exposure times than one hour at pH 1 or pH 13 will further deteriorate performance beneath practical use and should be tested.

We also developed a non-textured slippery copper surface that demonstrated high droplet mobility by creating a chemically and physically homogenous surface. Table 1 shows that there is room for improvement while thiolating copper surfaces. The surface could have better slipperiness by further reducing the R_{rms}. Chemical polishing methods could be optimized to decrease roughness before thiolation to improve performance as suggested by results from Table 1. Techniques for preventing/reducing oxidation could also be used to increase performance. Coating thickness will play a large role in applications such as condensation heat transfer due to the additional thermal conduction resistance. Thickness and the composition depth profile can be measured using Secondary Ion Mass Spectrometry (SIMS) while the surface chemistry can be evaluated using XPS. Oxidation of the surface could also be analyzed using vibrational sum frequency spectroscopy (VSFS), infrared reflection adsorption spectroscopy (IRAS) or cathodic reduction (CR).[46, 47] Performing condensation experiments to measure water collection rates and performing heat transfer experiments to compare heat transfer rates to plain copper can provide insights into the role of slipperiness in enhancing dropwise condensation. Promoters of droplet wise condensation heat transfer are known to increase heat transfer rates. Other promoters such as dioctadecyl disulfide and even relatively thick (few hundred μm) fluorocarbon coatings have been shown to increase heat transfer rates, but investigation using thiols and polished surfaces, to

the best of our knowledge, has not been explored.[44, 49-53] Other thiols could be investigated to try and find if other thiols that improve performance. Lifetime durability should also be investigated as it pertains to these applications, by determining the longevity of the coating under expected conditions.

REFERENCES

1. S. Pan, A. K. Kota, J. M. Mabry and A. Tuteja, *Journal of the American Chemical Society*, 2013, **135**, 578-581.
2. H. Vahabi, W. Wang, S. Movafaghi and A. K. Kota, *ACS Applied Materials & Interfaces*, 2016, **8**, 21962-21967.
3. H. F. Bohn and W. Federle, *Proceedings of the National Academy of Sciences of the United States of America*, 2004, **101**, 14138-14143.
4. H.-J. Butt, I. V. Roisman, M. Brinkmann, P. Papadopoulos, D. Vollmer and C. Semprebon, *Current Opinion in Colloid & Interface Science*, 2014, **19**, 343-354.
5. A. K. Kota, G. Kwon and A. Tuteja, *Npg Asia Materials*, 2014, **6**, e109.
6. T. Young, *Philosophical Transactions of the Royal Society of London*, 1805, **95**, 65-87.
7. A. B. D. Cassie and S. Baxter, *Transactions of the Faraday Society*, 1944, **40**, 546-551.
8. R. N. Wenzel, *Industrial & Engineering Chemistry*, 1936, **28**, 988-994.
9. E. Bittoun and A. Marmur, *Langmuir*, 2012, **28**, 13933-13942.
10. C. G. Furmidge, *Journal of Colloid Science*, 1962, **17**, 309-&.
11. S. T. Nguyen, J. Feng, N. T. Le, A. T. T. Le, N. Hoang, V. B. C. Tan and H. M. Duong, *Industrial & Engineering Chemistry Research*, 2013, **52**, 18386-18391.
12. D. Zheng, Y. Jiang, W. Yu, X. Jiang, X. Zhao, C.-H. Choi and G. Sun, *Langmuir*, 2017, **33**, 13640-13648.
13. R. E. Johnson and R. H. Dettre, *The Journal of Physical Chemistry*, 1964, **68**, 1744-1750.
14. R. H. Dettre and R. E. Johnson, in *Contact Angle, Wettability, and Adhesion*, AMERICAN CHEMICAL SOCIETY, 1964, vol. 43, ch. 8, pp. 136-144.

15. W. Wang, J. Salazar, H. Vahabi, A. Joshi-Imre, W. E. Voit and A. K. Kota, *Advanced Materials*, 2017, **29**, 1700295.

16. W. Wang, K. Lockwood, L. M. Boyd, M. D. Davidson, S. Movafaghi, H. Vahabi, S. R. Khetani and A. K. Kota, *ACS Applied Materials & Interfaces*, 2016, **8**, 18664-18668.

17. A. K. Kota, W. Choi and A. Tuteja, *MRS Bulletin*, 2013, **38**, 383-390.

18. L. Li, V. Breedveld and D. W. Hess, *ACS Appl Mater Interfaces*, 2013, **5**, 5381-5386.

19. H. Vahabi, W. Wang, K. C. Popat, G. Kwon, T. B. Holland and A. K. Kota, *Applied Physics Letters*, 2017, **110**, 251602.

20. A. Pendurthi, S. Movafaghi, W. Wang, S. Shadman, A. P. Yalin and A. K. Kota, *ACS Appl Mater Interfaces*, 2017, **9**, 25656-25661.

21. S. Movafaghi, W. Wang, A. Metzger, D. D. Williams, J. D. Williams and A. K. Kota, *Lab Chip*, 2016, **16**, 3204-3209.

22. S. Movafaghi, V. Leszczak, W. Wang, J. A. Sorkin, L. P. Dasi, K. C. Popat and A. K. Kota, *Advanced Healthcare Materials*, 2017, **6**, 1600717.

23. R. Enright, N. Miljkovic, N. Dou, Y. Nam and E. N. Wang, *Journal of Heat Transfer*, 2013, **135**, 091304-091304-091312.

24. N. Clegg, K. Kota, X. He and S. Ross, *Journal of Micro and Nano-Manufacturing*, 2017, **5**, 031003-031003-031007.

25. J. Zhang and S. Seeger, *Angew Chem Int Ed Engl*, 2011, **50**, 6652-6656.

26. C. Aulin, S. H. Yun, L. Wagberg and T. Lindstrom, *ACS Appl Mater Interfaces*, 2009, **1**, 2443-2452.

27. P. Phanthong, G. Guan, S. Karnjanakom, X. Hao, Z. Wang, K. Kusakabe and A. Abudula, *RSC Advances*, 2016, **6**, 13328-13334.

28. J. Li, L. Yan, Q. Ouyang, F. Zha, Z. Jing, X. Li and Z. Lei, *Chemical Engineering Journal*, 2014, **246**, 238-243.

29. C. Jin, Y. Jiang, T. Niu and J. Huang, *Journal of Materials Chemistry*, 2012, **22**, 12562.

30. L. Zhang, H. Kwok, X. Li and H. Z. Yu, *ACS Appl Mater Interfaces*, 2017, **9**, 39728-39735.

31. J. Wang, J. X. Wong, H. Kwok, X. Li and H. Z. Yu, *PLoS One*, 2016, **11**, e0151439.

32. L. Kong, Q. Wang, S. Xiong and Y. Wang, *Industrial & Engineering Chemistry Research*, 2014, **53**, 16516-16522.

33. P. Khanjani, A. W. T. King, G. J. Partl, L. S. Johansson, M. A. Kostiainen and R. H. A. Ras, *ACS Appl Mater Interfaces*, 2018, **10**, 11280-11288.

34. J. Huang, S. Wang and S. Lyu, *Materials (Basel)*, 2017, **10**.

35. M. Elsharkawy, T. M. Schutzius and C. M. Megaridis, *Lab Chip*, 2014, **14**, 1168-1175.

36. P. Dimitrakellis, A. Travlos, V. P. Psycharis and E. Gogolides, *Plasma Processes and Polymers*, 2017, **14**, 1600069.

37. L. Jiang, Z. Tang, R. M. Clinton, V. Breedveld and D. W. Hess, *ACS Appl Mater Interfaces*, 2017, **9**, 9195-9203.

38. F. Geyer, C. Schonecker, H. J. Butt and D. Vollmer, *Adv Mater*, 2017, **29**.

39. L. Wang and T. J. McCarthy, *Angewandte Chemie International Edition*, 2016, **55**, 244-248.

40. M. Boban, K. Golovin, B. Tobelmann, O. Gupte, J. M. Mabry and A. Tuteja, *ACS Applied Materials & Interfaces*, 2018, **10**, 11406-11413.

41. H. Tsuchiya, M. Tenjimbayashi, T. Moriya, R. Yoshikawa, K. Sasaki, R. Togasawa, T. Yamazaki, K. Manabe and S. Shiratori, *Langmuir*, 2017, **33**, 8950-8960.

42. H. Ron, H. Cohen, S. Matlis, M. Rappaport and I. Rubinstein, *The Journal of Physical Chemistry B*, 1998, **102**, 9861-9869.

43. C. A. Calderón, C. Ojeda, V. A. Macagno, P. Paredes-Olivera and E. M. Patrito, *The Journal of Physical Chemistry C*, 2010, **114**, 3945-3957.

44. C. Graham and P. Griffith, *International Journal of Heat and Mass Transfer*, 1973, **16**, 337-346.

45. N. Miljkovic, R. Enright and E. N. Wang, *ACS Nano*, 2012, **6**, 1776-1785.

46. S. Hosseinpour, M. Schwind, B. Kasemo, C. Leygraf and M. C. Johnson, *The Journal of Physical Chemistry C*, 2012, **116**, 24549-24557.

47. S. Hosseinpour, J. Hedberg, S. Baldelli, C. Leygraf and M. Johnson, *The Journal of Physical Chemistry C*, 2011, **115**, 23871-23879.

48. C. Teichert, J. F. MacKay, D. E. Savage, M. G. Lagally, M. Brohl and P. Wagner, *Applied Physics Letters*, 1995, **66**, 2346-2348.

49. J. W. Rose, *Proceedings of the Institution of Mechanical Engineers, Part A: Journal of Power and Energy*, 2002, **216**, 115-128.

50. X. Ma, J. W. Rose, D. Xu, J. Lin and B. Wang, *Chemical Engineering Journal*, 2000, **78**, 87-93.

51. C. E. Kirby, 1971.

52. A. Ghosh, S. Beaini, B. J. Zhang, R. Ganguly and C. M. Megaridis, *Langmuir*, 2014, **30**, 13103-13115.

53. S. Garg, *The effect of coatings and surfaces on dropwise condensation*, NAVAL CIVIL ENGINEERING LAB PORT HUENEME CA, 1969.

APPENDIX

A1. Statistical Analysis

Quantitative data was gathered and analyzed. To determine if the data was statistically different we determined if the data sets met the criteria and used one-way analysis of variance (ANOVA) tests were performed to determine if the difference was statistically significant. A 95% confidence interval (p-value = 0.05) was used to determine if the data was significant. If the test resulted in a p-value < 0.05 the two data sets were significantly different. All calculations were performed in Minitab 17 to determine which data sets were different.